

Nuclear lattice simulations with chiral effective field theoryDean Lee,¹ Buğra Borasoy,² and Thomas Schaefer^{1,3}¹*Physics Department, North Carolina State University, Raleigh, North Carolina 27695, USA*²*Physik Department, Technische Universität München D-85747, Garching, Germany*³*RIKEN-BNL Research Center, Brookhaven National Laboratory, Upton, New York 11973, USA*

(Received 2 March 2004; published 30 July 2004)

We study nuclear and neutron matter by combining chiral effective field theory with nonperturbative lattice methods. In our approach, nucleons and pions are treated as point particles on a lattice. This allows us to probe larger volumes, lower temperatures, and greater nuclear densities than in lattice QCD. The low-energy interactions of these particles are governed by chiral effective theory, and operator coefficients are determined by fitting to zero temperature few-body scattering data. The leading dependence on the lattice spacing can be understood from the renormalization group and absorbed by renormalizing operator coefficients. In this way, we have a realistic simulation of many-body nuclear phenomena with no free parameters, a systematic expansion, and a clear theoretical connection to QCD. We present results for hot neutron matter at temperatures 20–40 MeV and densities below twice the nuclear matter density.

DOI: 10.1103/PhysRevC.70.014007

PACS number(s): 21.30.Fe, 21.65+f, 13.75.Cs

I. INTRODUCTION

The nuclear many-body problem has long been recognized as one of the central questions in nuclear physics [1]. The traditional approach to the many-body problem is based on the assumption that nucleons can be treated as nonrelativistic point particles interacting mainly via two-body potentials. Three-body potentials, relativistic effects, and non-nucleonic degrees of freedom are assumed to give small corrections. The many-body problem is studied by solving the many-body Schrödinger equation. The ground-state properties of light nuclei and neutron drops have been analyzed by several groups using variational methods and Green's function Monte Carlo [2–7].

These methods have been very successful, but there are several good reasons for seeking an alternative approach. One reason is the desire for a theory that is more directly grounded in QCD. We expect this theory to explain why two-body forces are dominant, and how the interaction should be chosen. In addition to that, we would like to have a framework that allows the calculations to be systematically improved, and provides an estimate of the errors due to contributions that have been neglected. If we consider the interaction of a single nucleon with pions and external fields, such a framework is provided by chiral perturbation theory. In a very influential paper, Weinberg proposed to extend effective field theory methods to the nucleon-nucleon interaction [8]. Over the last several years, effective field theory methods have been applied successfully to the two- and three-nucleon system [9,10]. Effective field theory methods have also been applied to nuclear and neutron matter, but these calculations rely on a perturbative expansion in powers of the Fermi momentum [11,12].

Our aim in this work and the goal of the Nuclear Lattice Collaboration as a whole [13] is to extend effective field theory methods to the nuclear many-body problem. For this purpose we investigate the many-body physics of low-energy nucleons and pions on the lattice. Our starting point is the same as that of Weinberg. We begin with the most general

local Lagrangian involving pions and low-energy nucleons consistent with translational invariance, isospin symmetry, and spontaneously broken chiral symmetry. This yields an infinite set of possible interaction terms with increasing numbers of derivatives and/or nucleon fields. Degrees of freedom associated with antinucleons, heavier mesons such as the ρ , and heavier baryons such as the Δ , are integrated out. The contribution of these particles appear as coefficients of local terms in our pion-nucleon Lagrangian. We also integrate out nucleons with momenta greater than πa^{-1} , where a is the lattice spacing.

The operator coefficients in our effective Lagrangian are determined by fitting to experimentally measured few-body nucleon scattering data at zero temperature. The dependence on the lattice spacing is described by the renormalization group and can be absorbed by renormalizing operator coefficients. In this way, we construct a realistic simulation of many-body nuclear phenomena with no free parameters. In our discussion we present results for hot neutron matter at temperatures 20–40 MeV and densities below twice the nuclear matter density.

The first lattice study of nuclear matter was done by Brockmann and Frank [14]. They used a momentum lattice and analyzed the quantum hydrodynamics model of Walecka [15]. Müller *et al.* [16] were the first to look at infinite nuclear and neutron matter on a spatial lattice at finite density and temperature. They used an effective nucleon-nucleon interaction on a 4^3 lattice and found evidence for saturation in nuclear matter. The approach we pursue is similar in spirit to that of [16]. The main difference is the inclusion of pion degrees of freedom and our use of chiral effective field theory with Weinberg power counting. The nuclear liquid-gas transition has also been studied using classical lattice gas models [17–20].

II. NOTATION

Before describing the physics it will be helpful to first define the notation that we use throughout our discussion.

We let \vec{n} represent integer-valued lattice vectors on our 3 + 1 dimensional space-time lattice. We use a subscripted “s” such as in \vec{n}_s to represent purely spatial lattice vectors. We use subscripted indices such as i, j for the two spin components of the neutron, \uparrow and \downarrow . We let $\hat{0}$ be the unit lattice vector in the time direction and let $\hat{l}_s = \hat{1}, \hat{2}, \hat{3}$ be the corresponding unit lattice vectors in the spatial directions. A summation symbol such as

$$\sum_{l_s} \quad (1)$$

implies a summation over values $l_s = 1, 2, 3$.

We let a be the lattice spacing in the spatial direction and L be the length of the spatial lattice in each direction. a_t is the lattice spacing in the temporal direction and L_t is the length in the temporal direction. We let α_t be the ratio between lattice spacings,

$$\alpha_t = \frac{a_t}{a}. \quad (2)$$

Throughout, we use dimensionless parameters and operators, which correspond with physical values multiplied by the appropriate power of a . We use the superscript “phys” such as in m_N^{phys} to represent quantities with physical units. We use a, a^\dagger to represent annihilation and creation operators for the neutron, whereas c, c^* indicates the corresponding Grassmann variables in the path integral representation. We use the symbol: $f(a^\dagger, a)$: to indicate the normal ordering of operators in $f(a^\dagger, a)$. We let m_N be the mass of the neutron, μ be the neutron chemical potential, and m_π be the mass of the pion.

Our conventions for Fourier transforms are

$$\tilde{f}(\vec{k}) = \frac{1}{\sqrt{L_t L^3}} \sum_{\vec{n}} e^{i\vec{k} \cdot \vec{n}} f(\vec{n}), \quad (3)$$

$$f(\vec{n}) = \frac{1}{\sqrt{L_t L^3}} \sum_{\vec{k}} e^{-i\vec{k} \cdot \vec{n}} \tilde{f}(\vec{k}), \quad (4)$$

where

$$\vec{k}_* = \left(\frac{2\pi}{L_t} k_0, \frac{2\pi}{L} k_1, \frac{2\pi}{L} k_2, \frac{2\pi}{L} k_3 \right). \quad (5)$$

We use periodic boundary conditions in the spatial directions and periodic/antiperiodic boundary conditions in the temporal direction for bosons/fermions.

We let $D_N(\vec{k}) \delta_{ij}$ and $D_\pi(\vec{k})$ be the free neutron and neutral pion propagators. For notational convenience, the spin-conserving δ_{ij} in the neutron propagator will from here on be implicit. The self-energies, $\Sigma_N(\vec{k})$ and $\Sigma_\pi(\vec{k})$, are defined by

$$D_N^{\text{full}}(\vec{k}) = \frac{D_N(\vec{k})}{1 - \Sigma_N(\vec{k}) D_N(\vec{k})}, \quad (6)$$

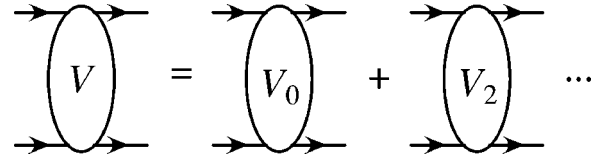


FIG. 1. Chiral expansion of the two-particle irreducible kernel.

$$D_\pi^{\text{full}}(\vec{k}) = \frac{D_\pi(\vec{k})}{1 - \Sigma_\pi(\vec{k}) D_\pi(\vec{k})}, \quad (7)$$

where $D_N^{\text{full}}(\vec{k})$ and $D_\pi^{\text{full}}(\vec{k})$ are the fully interacting propagators.

III. NONPERTURBATIVE EFFECTIVE FIELD THEORY

Effective field theory provides a systematic method to compute physical observables order by order in the small parameter Q/Λ_χ , where Λ_χ is the chiral symmetry breaking scale and $Q = (q, m_\pi, \dots)$. Here, q is a small external momentum and m_π is the mass of the pion. The simplest processes are those that involve only pions and external fields. In this case the effective field theory is perturbative. At any order in Q there are only a finite number of diagrams that have to be included. At lowest order these are tree diagrams with the leading-order interaction. At higher order, diagrams with more loops or higher-order terms in the interaction have to be taken into account.

Weinberg showed [8,21] that the simple diagrammatic expansion for nucleon-nucleon scattering is spoiled by infrared divergences. He suggested performing an expansion of the two-particle irreducible kernel (see Fig. 1) and then iterating the kernel to all orders to produce the scattering Green’s function (see Fig. 2). It was later pointed out that a possible difficulty arises because at any order in Q , an infinite number of diagrams is summed, and it is not clear that all the cutoff dependence at that order can be absorbed into counterterms that are present at that order [22]. This problem does indeed arise if one considers nucleon-nucleon scattering in the 1S_0 channel [23], but in practice the cutoff dependence appears to be very weak [24].

In this work we go one step further and consider the nuclear many-body problem. We expand the terms in our action order by order,

$$S = S_0 + S_1 + S_2 + \dots \quad (8)$$

At order k in the chiral expansion, we calculate observables by evaluating the functional integral

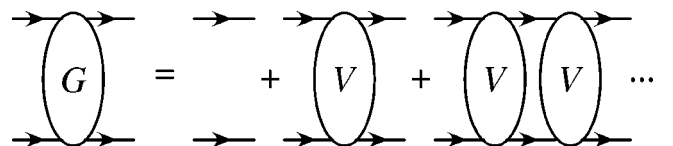


FIG. 2. The two-particle irreducible kernel is iterated to all orders to produce the nucleon-nucleon scattering Green’s function.

$$\begin{aligned} \langle G(\bar{N}, N, \pi) \rangle_k &= \frac{\int DND\bar{N}D\pi G(\bar{N}, N, \pi) \exp[-S_0 - S_1 - \dots - S_k]}{\int DND\bar{N}D\pi \exp[-S_0 - S_1 - \dots - S_k]}. \end{aligned} \quad (9)$$

We will refer to this approach as nonperturbative effective field theory. The interactions at chiral order k or less are iterated to arbitrary loop order. The functional integral is computed nonperturbatively by putting the pion and nucleon fields on the lattice and using Monte Carlo sampling. Since the number of diagrams at a given chiral order grows exponentially with the number of nucleons, a nonperturbative technique such as this is needed for systems with more than just a few nucleons.

Computing the path integral corresponds to summing an infinite set of diagrams. As in the case of iterating the two-particle irreducible kernel to determine the full two-nucleon Green's function, it is not clear that the cutoff dependence at a given order in the low-energy expansion can be absorbed into a finite number of coefficients in the action. In practice we will therefore restrict ourselves to lattice cutoffs that satisfy $\pi a^{-1} < \Lambda_\chi$. In order to show that the effective field theory calculation is consistent, we must find a window of lattice cutoffs such that the many-body calculation is independent of the cutoff up to terms that are higher order. We shall study this question numerically in our results section.

IV. LOWEST ORDER INTERACTIONS

Our momentum cutoff scale is πa^{-1} and we choose the lattice spacing so that

$$m_\pi < \pi a^{-1} < \Lambda_\chi. \quad (10)$$

An irreducible diagram is one that cannot be disconnected by cutting internal lines that match the set of incoming or outgoing particles. In the Weinberg counting scheme [8,21,25] we estimate the chiral order of an irreducible diagram by associating one power of Q/Λ_χ for each derivative interaction or explicit factor of m_π , four powers for each loop integral, one inverse power for each nucleon internal line, and two inverse powers for each pion internal line. If ν is the chiral order of an irreducible diagram, it can be shown that

$$\nu = 4 - \frac{e_n}{2} + 2l - 2c + \sum_{\text{vertex } i} \delta_i. \quad (11)$$

In Eq. (11), e_n is the number of external nucleons, l is the number of loops, c is the number of connected pieces, and δ_i for each vertex is

$$\delta_i = \#\partial + \#m_\pi + \frac{\#n}{2} - 2, \quad (12)$$

where $\#\partial$ is the number of derivatives, $\#m_\pi$ is the number of explicit factors of m_π in the coefficient, and $\#n$ is the number of nucleon fields. It turns out that $\#m_\pi$ is always an even number.

We let N represent the nucleon fields,

$$N = \begin{bmatrix} \text{proton} \\ \text{neutron} \end{bmatrix} \otimes \begin{bmatrix} \uparrow \\ \downarrow \end{bmatrix}. \quad (13)$$

We use τ_i to represent Pauli matrices acting in isospin space, and we use $\vec{\sigma}$ to represent Pauli matrices acting in spin space. Pion fields are notated as π_i . We denote the pion decay constant as $F_\pi^{phys} \approx 183$ MeV and let

$$D = 1 + \pi_i^2 / F_\pi^2. \quad (14)$$

The lowest-order Lagrange density for low-energy pions and nucleons is given by terms with $\delta_i=0$ [26],

$$\begin{aligned} \mathcal{L}^{(0)} = & -\frac{1}{2} D^{-2} [(\vec{\nabla} \pi_i)^2 - \dot{\pi}_i^2] - \frac{1}{2} D^{-1} m_\pi^2 \pi_i^2 \\ & + \bar{N} [i\partial_0 - (m_N - \mu)] N - D^{-1} F_\pi^{-1} g_A \bar{N} [\tau_i \vec{\sigma} \cdot \vec{\nabla} \pi_i] N \\ & - D^{-1} F_\pi^{-2} \bar{N} [\epsilon_{ijk} \tau_i \pi_j \dot{\pi}_k] N - \frac{1}{2} C_S \bar{N} N \bar{N} N \\ & - \frac{1}{2} C_T \bar{N} \vec{\sigma} N \cdot \bar{N} \vec{\sigma} N. \end{aligned} \quad (15)$$

g_A is the nucleon axial coupling and ϵ_{ijk} is the Levi-Civita symbol. The chemical potential μ controls the nucleon density and μ will be set very close to m_N . At next order we have terms with $\delta_i=1$,

$$\mathcal{L}^{(1)} = \frac{1}{2m_N} \bar{N} \vec{\nabla}^2 N + \dots \quad (16)$$

We will include this kinetic energy term from $\mathcal{L}^{(1)}$ in our lowest-order Lagrange density so that we get the usual free nucleon propagator.

In this study we limit ourselves to the interactions of neutrons and neutral pions and consider processes with only up to two pions. As a result we have at lowest order the terms

$$\begin{aligned} \mathcal{L} = & -\frac{1}{2} [-\dot{\pi}_0^2 + (\vec{\nabla} \pi_0)^2 + m_\pi^2 \pi_0^2] + a_j^\dagger \left[i\partial_0 + \frac{\vec{\nabla}^2}{2m_N} \right. \\ & \left. - (m_N - \mu) \right] a_j + \frac{g_A}{F_\pi} a_i^\dagger \vec{\sigma}_{ij} a_j \cdot \vec{\nabla} \pi_0 - C a_i^\dagger a_1 a_1^\dagger a_i, \end{aligned} \quad (17)$$

where a, a^\dagger are annihilation and creation operators for the neutron. In the Euclidean formalism, we have the partition function

$$Z = \int D\pi DND\bar{N} \exp(-S_E) = \int D\pi DND\bar{N} \exp\left(\int d^4x \mathcal{L}_E\right), \quad (18)$$

where

$$\mathcal{L}_E = -\frac{1}{2}[\dot{\vec{\pi}}_0^2 + (\vec{\nabla} \pi_0)^2 + m_\pi^2 \pi_0^2] - a_j^\dagger \left[\partial_0 - \frac{\vec{\nabla}^2}{2m_N} + (m_N - \mu) \right] a_j + \frac{g_A}{F_\pi} a_i^\dagger \vec{\sigma}_{ij} a_j \cdot \vec{\nabla} \pi_0 - C a_i^\dagger a_{i+1}^\dagger a_{i+1} a_i. \quad (19)$$

We will use x_0 to represent the Euclidean temporal coordinate, rather than switching from x_0 to x_4 .

V. FREE NEUTRON

In the simplest discretization, the Euclidean lattice action for free neutrons has the form

$$S_{NN}^{\text{simple}} = \sum_{\vec{n}, i} [c_i^*(\vec{n}) c_i(\vec{n} + \hat{0}) + (-1 + (m_N - \mu) \alpha_t c_i^*(\vec{n}) c_i(\vec{n})] - h \sum_{\vec{n}, \hat{l}_s, i} [c_i^*(\vec{n}) c_i(\vec{n} + \hat{l}_s) + c_i^*(\vec{n}) c_i(\vec{n} - \hat{l}_s)], \quad (20)$$

where

$$h = \frac{\alpha_t}{2m_N}. \quad (21)$$

However, we want a discretization that will minimize the dependence on α_t so that fewer lattice steps in the temporal direction can be used, and results for different α_t can be directly compared.

Let us review the conversion from the operator formalism to path integrals. The free neutron lattice Hamiltonian is

$$H_{NN}^- = \sum_{\vec{n}, i} \left[\left(m_N - \mu + \frac{3}{m_N} \right) a_i^\dagger(\vec{n}_s) a_i(\vec{n}_s) \right] - \frac{1}{2m_N} \sum_{\vec{n}_s, \hat{l}_s, i} [a_i^\dagger(\vec{n}_s) a_i(\vec{n}_s + \hat{l}_s) + a_i^\dagger(\vec{n}_s) a_i(\vec{n}_s - \hat{l}_s)]. \quad (22)$$

We want to convert the partition function for free neutrons,

$$Z = \text{Tr}[\exp(-\beta H_{NN}^-)] = \text{Tr}[\exp(-\alpha_t H_{NN}^-) \exp(-\alpha_t H_{NN}^-) \dots \exp(-\alpha_t H_{NN}^-)], \quad (23)$$

into the form

$$Z = \int Dc Dc^* \exp[-S_{NN}^-]. \quad (24)$$

Using the identity [27]

$$\exp[a_i^\dagger X_{ij} a_j] =: \exp[a_i^\dagger (e^X - 1)_{ij} a_j] :, \quad (25)$$

we can write

$$\exp(-\alpha_t H_{NN}^-) =: \exp[-h_{NN}^-(a^\dagger, a)] : + O(h), \quad (26)$$

where

$$h_{NN}^-(a^\dagger, a) = \sum_{\vec{n}_s, i} [(1 - e^{-(m_N - \mu)\alpha_t + 6h}) a_i^\dagger(\vec{n}_s) a_i(\vec{n}_s)] - h e^{-(m_N - \mu)\alpha_t} \sum_{\vec{n}_s, \hat{l}_s, i} [a_i^\dagger(\vec{n}_s) a_i(\vec{n}_s + \hat{l}_s) + a_i^\dagger(\vec{n}_s) a_i(\vec{n}_s - \hat{l}_s)]. \quad (27)$$

Introducing the extra $e^{-(m_N - \mu)\alpha_t}$ factor multiplying h is not well motivated at this stage, but it insures that the neutron chemical potential is coupled to an exactly conserved neutron number operator [28,29]. We now use the correspondence [27,30]

$$\text{Tr}[:f_{n-1}(a^\dagger, a) : \dots :f_1(a^\dagger, a) : : f_0(a^\dagger, a) :] = \int dc_{n-1} dc_{n-1}^* \dots dc_0 dc_0^* \times \exp\left[\sum_{j=0, \dots, n-1} c_j^*(c_j - c_{j+1}) \right] \prod_{j=0, \dots, n-1} f_j(c_j^*, c_j), \quad (28)$$

with $c_n = -c_0$. We can now convert the partition function to the path integral form in Eq. (24) with

$$S_{NN}^- = \sum_{\vec{n}_s, i} [c_i^*(\vec{n}) c_i(\vec{n} + \hat{0}) - e^{-(m_N - \mu)\alpha_t + 6h} c_i^*(\vec{n}) c_i(\vec{n})] - h e^{-(m_N - \mu)\alpha_t} \sum_{\vec{n}_s, \hat{l}_s, i} [c_i^*(\vec{n}) c_i(\vec{n} + \hat{l}_s) + c_i^*(\vec{n}) c_i(\vec{n} - \hat{l}_s)]. \quad (29)$$

This lattice action has temporal discretization errors of $O(h)$, whereas the action in Eq. (20) has errors of $O(\alpha_t)$. Since h is a small parameter, this is an improvement and so the dependence on α_t has been significantly reduced.

It is conventional to define a new normalization for c_i ,

$$c_i' = c_i e^{-(m_N - \mu)\alpha_t}. \quad (30)$$

Then

$$Z = e^{-2(m_N - \mu)\beta L^3} \int Dc' Dc^* \exp[-S_{NN}^-], \quad (31)$$

where

$$S_{NN}^- = \sum_{\vec{n}, i} [e^{(m_N - \mu)\alpha_t} c_i^*(\vec{n}) c_i'(\vec{n} + \hat{0}) - e^{-6h} c_i^*(\vec{n}) c_i'(\vec{n})] - h \sum_{\vec{n}_s, \hat{l}_s, i} [c_i^*(\vec{n}) c_i'(\vec{n} + \hat{l}_s) + c_i^*(\vec{n}) c_i'(\vec{n} - \hat{l}_s)]. \quad (32)$$

We observe that the neutron chemical potential is in fact coupled to an exactly conserved neutron number operator since it appears in the same manner as a lattice gauge connection in the temporal direction. Comparing the two actions (20) and (32), we can summarize the difference as follows. If we write

$$\begin{aligned}
 S_{NN}^{\text{simple}} = & \sum_{\vec{n},i} [c_i^*(\vec{n})c_i(\vec{n} + \hat{0})] + \sum_{\vec{n},i} [(-1 + (m_N - \mu)\alpha_t + X \\
 & \times c_i^*(\vec{n})c_i(\vec{n})] - h \sum_{\vec{n},\hat{l}_s,i} [c_i^*(\vec{n})c_i(\vec{n} + \hat{l}_s) \\
 & + c_i^*(\vec{n})c_i(\vec{n} - \hat{l}_s)], \quad (33)
 \end{aligned}$$

where

$$X = 6h, \quad (34)$$

then

$$\begin{aligned}
 S_{NN}^- = & \sum_{\vec{n},i} [e^{(m_N - \mu)\alpha_t} c_i^*(\vec{n})c_i'(\vec{n} + \hat{0})] - \sum_{\vec{n},i} [c_i^*(\vec{n})e^{-X}c_i'(\vec{n})] \\
 & - h \sum_{\vec{n},\hat{l}_s,i} [c_i^*(\vec{n})c_i'(\vec{n} + \hat{l}_s) + c_i^*(\vec{n})c_i'(\vec{n} - \hat{l}_s)]. \quad (35)
 \end{aligned}$$

In momentum space we have

$$\begin{aligned}
 S_{NN}^- = & \sum_{\vec{k},i} \tilde{c}_i^*(-\vec{k})\tilde{c}_i'(\vec{k}) \left[e^{-ik_0 + (m_N - \mu)\alpha_t} - e^{-6h} \right. \\
 & \left. - 2h \sum_{\hat{l}_s} \cos(k_{*l_s}) \right]. \quad (36)
 \end{aligned}$$

We now have the free neutron correlation function on the lattice,

$$\frac{\int Dc' Dc^* c_i'(\vec{n})c_i^*(0)\exp[-S_{NN}^-]}{\int Dc' Dc^* \exp[-S_{NN}^-]} = \frac{1}{L_t L^3} \sum_{\vec{k}} e^{-ik_0 \cdot \vec{n}} D_N(\vec{k}), \quad (37)$$

(no sum over i) where the free neutron propagator is

$$D_N(\vec{k}) = \frac{1}{e^{-ik_0 + (m_N - \mu)\alpha_t} - e^{-6h} - 2h \sum_{\hat{l}_s} \cos(k_{*l_s})}. \quad (38)$$

VI. NEUTRON CORRELATION FUNCTIONS

At a nonzero time step there are some subtleties going from the correlation functions in the operator formalism to correlation functions in the path integral formalism. We have

$$\begin{aligned}
 Z = & \text{Tr}[\exp(-\alpha_t H) \dots \exp(-\alpha_t H)\exp(-\alpha_t H)] \\
 = & \text{Tr}[:f_{L_t-1}(a^\dagger, a) : \dots :f_1(a^\dagger, a) : : f_0(a^\dagger, a) :], \quad (39)
 \end{aligned}$$

where the total number of time steps is L_t and each of the f_j 's are the same,

$$:f_j(a^\dagger, a) : = \exp(-\alpha_t H) + O(h). \quad (40)$$

Suppose we wish to calculate

$$\text{Tr}[u_{L_t-1}(a)v_{L_t-1}(a^\dagger):f_{L_t-1}:\dots:u_1(a)v_1(a^\dagger):f_1:u_0(a)v_0(a^\dagger):f_0:]. \quad (41)$$

This can be rewritten as

$$\begin{aligned}
 \text{Tr}[:v_{L_t-1}(a^\dagger)f_{L_t-1}u_{L_t-2}(a):\dots:v_1(a^\dagger)f_1u_0(a) : : v_0(a^\dagger) \\
 \times f_0u_{L_t-1}(a) :]. \quad (42)
 \end{aligned}$$

In the path integral formalism this is equivalent to

$$\int Dc Dc^* F(c, c^*) \exp[-S], \quad (43)$$

where

$$F(c, c^*) = v_{L_t-1}(c_{L_t-1}^*)u_{L_t-2}(c_{L_t-1}) \dots v_0(c_0^*)u_{L_t-1}(c_0). \quad (44)$$

We note that v_j is a function of c_j , whereas u_j is a function of c_{j+1} .

VII. FREE NEUTRAL PION

The lattice action for a free neutral pion is

$$\begin{aligned}
 S_{\pi\pi} = & \left[\left(\frac{m_\pi^2}{2} + 3 \right) \alpha_t + \alpha_t^{-1} \right] \sum_{\vec{n}} \pi(\vec{n})\pi(\vec{n}) \\
 & - \sum_{\vec{n},\hat{l}} [e_l \pi(\vec{n})\pi(\vec{n} + \hat{l})], \quad (45)
 \end{aligned}$$

where

$$(e_0, e_1, e_2, e_3) = (\alpha_t^{-1}, \alpha_t, \alpha_t, \alpha_t). \quad (46)$$

In momentum space the action is

$$S_{\pi\pi} = \sum_{\vec{n}} \pi(-\vec{k})\pi(\vec{k}) \left[\left(\frac{m_\pi^2}{2} + 3 \right) \alpha_t + \alpha_t^{-1} - \sum_{\hat{l}} e_l \cos(k_{*l}) \right], \quad (47)$$

and so

$$\frac{\int D\pi \pi(\vec{n})\pi(0)\exp[-S_{\pi\pi}]}{\int D\pi \exp[-S_{\pi\pi}]} = \frac{1}{L_t L^3} \sum_{\vec{k}} e^{-ik_0 \cdot \vec{n}} D_\pi(\vec{k}), \quad (48)$$

where the free neutral pion propagator is

$$D_\pi(\vec{k}) = \frac{1}{2 \left[\left(\frac{m_\pi^2}{2} + 3 \right) \alpha_t + \alpha_t^{-1} - \sum_{\hat{l}} e_l \cos(k_{*l}) \right]}. \quad (49)$$

In this first exploratory study we are not concerned with the issue of exact chiral symmetry on the lattice and therefore will neglect the Haar measure. This aspect of exact chiral symmetry will be investigated in a future study along with the inclusion of charged nucleons and pions.

VIII. NEUTRAL PION-NEUTRON COUPLING

In the continuum, the pion-nucleon coupling makes a contribution to the integrand of the partition function of the form

$$\exp\left[-\frac{g_A}{F_\pi}\int d^4x D^{-1}\bar{N}[\vec{\tau}_a(\vec{\sigma}\cdot\vec{\nabla}\pi_a)]N\right], \quad (50)$$

where $\vec{\sigma}=(\sigma_1,\sigma_2,\sigma_3)$ are Pauli matrices for spin, $\tau_a=(\tau_1,\tau_2,\tau_3)$ are Pauli matrices for isospin,

$$D=1+\frac{\vec{\pi}^2}{F_\pi^2}, \quad (51)$$

and $F_\pi^{phys}\approx 183$ MeV is the pion decay constant,

$$\langle 0|j_{5a}^\mu|\pi_b(p)\rangle=i\delta_{ab}\frac{F_\pi}{2}p^\mu. \quad (52)$$

We keep only the term involving the neutral pion and neutron,

$$\exp\left[\frac{g_A}{F_\pi}\int d^4x(c_i^*\vec{\sigma}_{ij}c_j\cdot\vec{\nabla}\pi_0)\right]. \quad (53)$$

The simplest lattice discretization of this interaction term is

$$\exp[-S_{\pi\bar{N}N}], \quad (54)$$

where

$$\begin{aligned} S_{\pi\bar{N}N}^{\text{simple}} &= -\frac{g_A\alpha_t}{2F_\pi}\sum_{\vec{n}}\{[c_\uparrow^*(\vec{n})c_\uparrow(\vec{n})-c_\downarrow^*(\vec{n})c_\downarrow(\vec{n})]\Delta_3^\pm\pi_0(\vec{n})\} \\ &\quad -\frac{g_A\alpha_t}{2F_\pi}\sum_{\vec{n}}\{c_\uparrow^*(\vec{n})c_\downarrow(\vec{n})[\Delta_1^\pm\pi_0(\vec{n})-i\Delta_2^\pm\pi_0(\vec{n})]\} \\ &\quad -\frac{g_A\alpha_t}{2F_\pi}\sum_{\vec{n}}\{c_\downarrow^*(\vec{n})c_\uparrow(\vec{n})[\Delta_1^\pm\pi_0(\vec{n})+i\Delta_2^\pm\pi_0(\vec{n})]\}. \end{aligned} \quad (55)$$

and

$$\Delta_l^\pm\pi_0(\vec{n})=\pi_0(\vec{n}+\hat{l})-\pi_0(\vec{n}-\hat{l}). \quad (56)$$

We now use a temporally improved discretization. We can write the simple lattice action for the free neutron with pion-neutron coupling as

$$\begin{aligned} S_{\bar{N}N}^{\text{simple}}+S_{\pi\bar{N}N}^{\text{simple}} &= \sum_{\vec{n},i}c_i^*(\vec{n})c_i(\vec{n}+\hat{0}) \\ &\quad +\sum_{\vec{n},i,j}c_i^*(\vec{n})\{[-1+(m_N-\mu)\alpha_t]\delta_{ij} \\ &\quad +X_{ij}(\vec{n})\}c_j(\vec{n})-h\sum_{\vec{n},\hat{l}_s,i}[c_i^*(\vec{n})c_i(\vec{n}+\hat{l}_s) \\ &\quad +c_i^*(\vec{n})c_i(\vec{n}-\hat{l}_s)], \end{aligned} \quad (57)$$

with $X_{ij}(\vec{n})$ given by the matrix

$$\begin{bmatrix} 6h-\frac{g_A\alpha_t}{2F_\pi}\Delta_3^\pm\pi_0(\vec{n}) & -\frac{g_A\alpha_t}{2F_\pi}(\Delta_1^\pm-i\Delta_2^\pm)\pi_0(\vec{n}) \\ -\frac{g_A\alpha_t}{2F_\pi}(\Delta_1^\pm+i\Delta_2^\pm)\pi_0(\vec{n}) & 6h+\frac{g_A\alpha_t}{2F_\pi}\Delta_3^\pm\pi_0(\vec{n}) \end{bmatrix}. \quad (58)$$

Then our temporally improved action is

$$\begin{aligned} S_{\bar{N}N+\pi\bar{N}N} &= \sum_{\vec{n},i}e^{(m_N-\mu)\alpha_t}c_i^*(\vec{n})c_i'(\vec{n}+\hat{0})-\sum_{\vec{n},i,j}c_i^*(\vec{n}) \\ &\quad \times(e^{-X(\vec{n})})_{ij}c_j'(\vec{n})-h\sum_{\vec{n},\hat{l}_s,i}[c_i^*(\vec{n})c_i'(\vec{n}+\hat{l}_s) \\ &\quad +c_i^*(\vec{n})c_i'(\vec{n}-\hat{l}_s)]. \end{aligned} \quad (59)$$

IX. NEUTRON CONTACT TERM

The neutron contact term has the form

$$H_{\bar{N}N\bar{N}N}=C\sum_{\vec{n},i}a_\uparrow^\dagger(\vec{n})a_\uparrow(\vec{n})a_\downarrow^\dagger(\vec{n})a_\downarrow(\vec{n}). \quad (60)$$

We can rewrite the contribution at lattice site \vec{n} to the partition function using a discrete Hubbard-Stratonovich transformation [31]. For $C\leq 0$,

$$\begin{aligned} &\exp[-C\alpha_t a_\uparrow^\dagger(\vec{n})a_\uparrow(\vec{n})a_\downarrow^\dagger(\vec{n})a_\downarrow(\vec{n})] \\ &= \frac{1}{2}\sum_{s(\vec{n})=\pm 1}\exp\left\{-\left[\frac{C\alpha_t}{2}+\lambda s(\vec{n})\right]\right. \\ &\quad \left.\times[a_\uparrow^\dagger(\vec{n})a_\uparrow(\vec{n})+a_\downarrow^\dagger(\vec{n})a_\downarrow(\vec{n})-1]\right\}, \end{aligned} \quad (61)$$

where

$$\cosh\lambda=\exp\left(-\frac{C\alpha_t}{2}\right). \quad (62)$$

Since

$$e^\lambda+e^{-\lambda}=2\exp\left(-\frac{C\alpha_t}{2}\right), \quad (63)$$

we can write

$$\lambda=\ln\left[\exp\left(-\frac{C\alpha_t}{2}\right)+\sqrt{\exp(-C\alpha_t)-1}\right]. \quad (64)$$

The simplest lattice discretization gives a contribution to action,

$$-\frac{C\beta}{2}L^3 + S_{ss} + S_{sNN}^{\text{simple}}, \quad (65)$$

where

$$S_{ss} = -\sum_{\vec{n}} \lambda s(\vec{n}) \quad (66)$$

and

$$S_{sNN}^{\text{simple}} = \sum_{\vec{n}} \left\{ \left[\frac{C\alpha_t}{2} + \lambda s(\vec{n}) \right] [c_{\uparrow}^*(\vec{n})c_{\uparrow}(\vec{n}) + c_{\downarrow}^*(\vec{n})c_{\downarrow}(\vec{n})] \right\}. \quad (67)$$

However, this actually gives a result that is inconsistent with the Hamiltonian operator form in Eq. (61) in limit $\alpha_t \rightarrow 0$. The problem is somewhat subtle and has not been given

much attention in the literature. The point is that operator ordering at $O(\lambda^2)$ cannot be ignored since $\lambda^2 \sim O(\alpha_t)$. We will deal with this in the same way that we constructed the temporally improved action for the free neutron and the pion-neutron coupling. We write

$$\begin{aligned} S_{NN}^{\text{simple}} + S_{\pi NN}^{\text{simple}} + S_{sNN}^{\text{simple}} \\ = \sum_{\vec{n},i} c_i^*(\vec{n})c_i(\vec{n} + \hat{0}) + \sum_{\vec{n},i,j} c_i^*(\vec{n})\{-1 + (m_N - \mu)\alpha_t\}\delta_{ij} \\ + X_{ij}(\vec{n})\}c_j(\vec{n}) - h \sum_{\vec{n},\hat{l}_s,i} [c_i^*(\vec{n})c_i(\vec{n} + \hat{l}_s) + c_i^*(\vec{n})c_i(\vec{n} - \hat{l}_s)], \end{aligned} \quad (68)$$

with $X_{ij}(\vec{n})$ equal to

$$\left[\begin{array}{l} 6h - \frac{g_A\alpha_t}{2F_\pi}\Delta_3^\pm\pi_0(\vec{n}) + \frac{C\alpha_t}{2} + \lambda s(\vec{n}) \\ - \frac{g_A\alpha_t}{2F_\pi}(\Delta_1^\pm - i\Delta_2^\pm)\pi_0(\vec{n}) \\ - \frac{g_A\alpha_t}{2F_\pi}(\Delta_1^\pm + i\Delta_2^\pm)\pi_0(\vec{n}) \\ 6h + \frac{g_A\alpha_t}{2F_\pi}\Delta_3^\pm\pi_0(\vec{n}) + \frac{C\alpha_t}{2} + \lambda s(\vec{n}) \end{array} \right], \quad (69)$$

then

$$\begin{aligned} S_{NN+\pi NN+sNN}^{\bar{}} = \sum_{\vec{n},i} e^{(m_N-\mu)\alpha_t} c_i^*(\vec{n})c_i'(\vec{n} + \hat{0}) - \sum_{\vec{n},i,j} c_i^*(\vec{n}) \\ \times (e^{-X(\vec{n})})_{ij} c_j'(\vec{n}) - h \sum_{\vec{n},\hat{l}_s,i} [c_i^*(\vec{n})c_i(\vec{n} + \hat{l}_s) \\ + c_i^*(\vec{n})c_i(\vec{n} - \hat{l}_s)]. \end{aligned} \quad (70)$$

X. ONE-LOOP NEUTRON SELF-ENERGY

In the next few sections we calculate several lattice Feynman diagrams. These calculations will serve as a check that our nonperturbative simulation is functioning properly in the small coupling limit $g_A \rightarrow 0$, $C \rightarrow 0$. It will also give us a reference point to measure how nonperturbative the interactions are at physical values for g_A and C and for various densities.

At $O(g_A^2)$ we have a contribution to the neutron self-energy due to a neutral pion and neutron intermediate state,

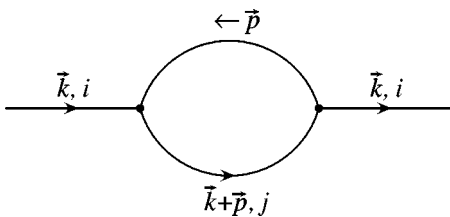


FIG. 3. Neutron self-energy due to a neutral pion and neutron intermediate state.

as shown in Fig. 3. If we write the pion-nucleon interaction term to order $O(g_A)$ in momentum space, we have a contribution to the action of the form

$$\begin{aligned} \frac{ig_A\alpha_t e^{-6h}}{F_\pi\sqrt{L^3}L_t} \sum_{\vec{k},\vec{p}} [\tilde{c}_{\uparrow}^*(-\vec{k}-\vec{p})\tilde{c}'_{\uparrow}(\vec{k}) - \tilde{c}_{\downarrow}^*(-\vec{k}-\vec{p})\tilde{c}'_{\downarrow}(\vec{k})] \pi_0(\vec{p}) \\ \times \sin(p_{*3}) + \frac{ig_A\alpha_t e^{-6h}}{F_\pi\sqrt{L^3}L_t} \\ \times \sum_{\vec{k},\vec{p}} [\tilde{c}_{\uparrow}^*(-\vec{k}-\vec{p})\tilde{c}'_{\downarrow}(\vec{k})] \pi_0(\vec{p}) [\sin(p_{*1}) - i\sin(p_{*2})] \\ + \frac{ig_A\alpha_t e^{-6h}}{F_\pi\sqrt{L^3}L_t} \sum_{\vec{k},\vec{p}} [\tilde{c}_{\downarrow}^*(-\vec{k}-\vec{p})\tilde{c}'_{\uparrow}(\vec{k})] \pi_0(\vec{p}) [\sin(p_{*1}) \\ + i\sin(p_{*2})]. \end{aligned} \quad (71)$$

Then the diagram in Fig. 3 leads to a contribution to the self-energy that goes as

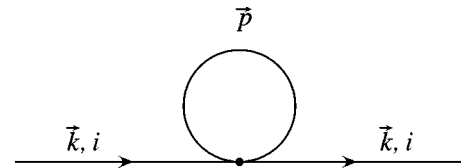


FIG. 4. Neutron self-energy due to the $\pi\pi\bar{N}N$ interaction in the temporally improved action.

$$\Sigma_N^{(g_A^2)}(\vec{k}) = \frac{g_A^2 \alpha_t^2 e^{-12h}}{F_\pi^2 L^3 L_t} \sum_{\vec{p}} D_\pi(\vec{p}) D_N(\vec{k} + \vec{p}) [\sin^2(p_{*1}) + \sin^2(p_{*2}) + \sin^2(p_{*3})]. \quad (72)$$

Our temporally improved action has a $\pi\pi\bar{N}N$ interaction of the form

$$S = \dots - \frac{g_A^2 \alpha_t^2}{8F_\pi^2} e^{-6h} \sum_{\vec{n}, \hat{i}, s} c_i^*(\vec{n}) c'_i(\vec{n}) [\Delta_{i_s}^\pm \pi_0(n)]^2, \quad (73)$$

which gives rise to the diagram in Fig. 4. We get an additional contribution to the self-energy,

$$\Sigma_N^{(g_A^2)}(\vec{k}) = \dots + \frac{g_A^2 \alpha_t^2}{8F_\pi^2} e^{-6h} X, \quad (74)$$

where

$$\frac{1}{2} \sum_{s(\vec{n})=\pm 1} e^{(C\alpha_t/2+\lambda s(\vec{n}))} \exp[e^{-6h}(e^{-[C\alpha_t/2+\lambda s(\vec{n})]} - 1)(c_\uparrow^*(\vec{n})c'_\uparrow(\vec{n}) + c_\downarrow^*(\vec{n})c'_\downarrow(\vec{n}))]. \quad (76)$$

Expanding the exponential, we get

$$\frac{1}{2} \sum_{s(\vec{n})=\pm 1} e^{[C\alpha_t/2+\lambda s(\vec{n})]} \left\{ \begin{aligned} &1 + e^{-6h}(e^{-[C\alpha_t/2+\lambda s(\vec{n})]} - 1)[c_\uparrow^*(\vec{n})c'_\uparrow(\vec{n}) + c_\downarrow^*(\vec{n})c'_\downarrow(\vec{n})] \\ &+ e^{-12h}(e^{-[C\alpha_t/2+\lambda s(\vec{n})]} - 1)^2 c_\uparrow^*(\vec{n})c'_\uparrow(\vec{n})c_\downarrow^*(\vec{n})c'_\downarrow(\vec{n}) \end{aligned} \right\}. \quad (77)$$

We find that

$$\frac{1}{2} \sum_{s(\vec{n})=\pm 1} e^{[C\alpha_t/2+\lambda s(\vec{n})]} (e^{-[C\alpha_t/2+\lambda s(\vec{n})]} - 1) = 0 \quad (78)$$

and

$$\frac{1}{2} \sum_{s(\vec{n})=\pm 1} e^{[C\alpha_t/2+\lambda s(\vec{n})]} (e^{-[C\alpha_t/2+\lambda s(\vec{n})]} - 1)^2 = e^{-C\alpha_t} - 1. \quad (79)$$

So to lowest order, we can write the interaction as

$$e^{-12h}(e^{-C\alpha_t} - 1)c_\uparrow^*(\vec{n})c'_\uparrow(\vec{n})c_\downarrow^*(\vec{n})c'_\downarrow(\vec{n}). \quad (80)$$

Therefore, the contribution to the self-energy is

$$\Sigma_N^{(C)}(\vec{k}) = e^{-12h}(e^{-C\alpha_t} - 1)Y, \quad (81)$$

where

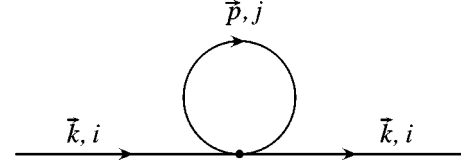


FIG. 5. Neutron self-energy due to the contact interaction.

$$X = \frac{4}{L_t L^3} \sum_{\vec{p}} D_\pi(\vec{p}) [\sin^2(p_{*1}) + \sin^2(p_{*2}) + \sin^2(p_{*3})]. \quad (75)$$

At $O(C)$ we have the one-loop diagram shown in Fig. 5. If the vertex is located at lattice site \vec{n} , we can isolate the relevant lowest-order interaction in the path integral starting from

$$Y = \frac{\int Dc' Dc^* c_i^*(0) c'_i(0) \exp[-S_{\bar{N}N}]}{\int Dc' Dc^* \exp[-S_{\bar{N}N}]} \text{(no sum over } i) \\ = -\frac{1}{L_t L^3} \sum_{\vec{k}} D_N(\vec{k}). \quad (82)$$

This self-energy term is proportional to Y , which in turn is proportional to the neutron density with an $O(\alpha_t)$ time discretization correction.

XI. ONE-LOOP PION SELF-ENERGY

At $O(g_A^2)$ we have a contribution to the pion self-energy due to a neutron and neutron-hole intermediate state, as shown in Fig. 6. The contribution to the self-energy is

$$\Sigma_\pi^{(g_A^2)}(\vec{k}) = -\frac{2g_A^2 \alpha_t^2 e^{-12h}}{F_\pi^2 L^3 L_t} \sum_{\vec{p}} D_N(\vec{p}) D_N(\vec{k} + \vec{p}) \\ \times [\sin^2(k_{*1}) + \sin^2(k_{*2}) + \sin^2(k_{*3})], \quad (83)$$

Our temporally improved action has a term of the form

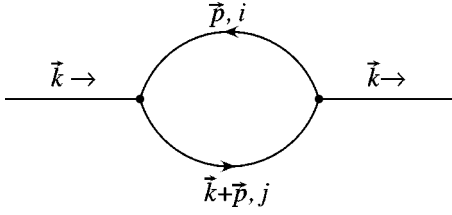


FIG. 6. Pion self-energy due to neutron-neutron hole intermediate states.

$$S = \dots - \frac{g_A^2 \alpha_t^2}{8F_\pi^2} e^{-6h} \sum_{\vec{n}, \hat{l}_{s,i}} c_i^*(\vec{n}) c_i'(\vec{n}) [\Delta_{l_s}^\pm \pi_0(n)]^2. \quad (84)$$

This leads to the diagram in Fig. 7 and gives an additional contribution

$$\Sigma_\pi^{(g_A^2)}(\vec{k}) = \dots + \frac{2g_A^2 \alpha_t^2}{F_\pi^2} e^{-6h} Y [\sin^2(k_{*1}) + \sin^2(k_{*2}) + \sin^2(k_{*3})]. \quad (85)$$

XII. TWO-LOOP AVERAGE ENERGY

We will calculate the shift in the average energy by computing

$$-\frac{\partial}{\partial \beta} \ln \left[\frac{Z(g_A^2, C)}{Z(0, 0)} \right]. \quad (86)$$

The logarithm of the full partition function is the sum of the connected diagrams. At $O(g_A^2)$, we get a contribution from the connected bubble diagram shown in Fig. 8.

The amplitude for this bubble can be obtained in a straightforward manner from either Eq. (72) and (83):

$$-\frac{g_A^2 \alpha_t^2 e^{-12h}}{F_\pi^2 L^3 L_t} \sum_{\vec{p}, \vec{k}} D_N(\vec{p}) D_N(\vec{k} + \vec{p}) D_\pi(\vec{k}) [\sin^2(k_{*1}) + \sin^2(k_{*2}) + \sin^2(k_{*3})]. \quad (87)$$

In our temporally improved action the term

$$S = \dots - \frac{g_A^2 \alpha_t^2}{8F_\pi^2} e^{-6h} \sum_{\vec{n}, \hat{l}_{s,i}} c_i^*(\vec{n}) c_i'(\vec{n}) [\Delta_{l_s}^\pm \pi_0(n)]^2. \quad (88)$$

produces the diagram shown in Fig. 9. The amplitude for this process can be computed from either Eq. (74) or (85) and is

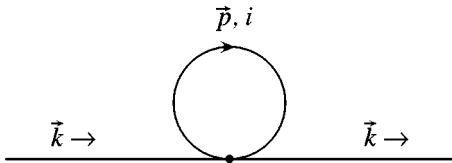


FIG. 7. Pion self-energy due to the $\pi\pi\bar{N}\bar{N}$ interaction in the temporally improved action.

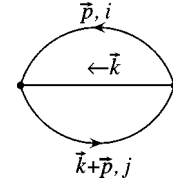


FIG. 8. Two-loop connected bubble diagram at $O(g_A^2)$.

$$\begin{aligned} & \frac{g_A^2 \alpha_t^2}{F_\pi^2} e^{-6h} Y \sum_{\vec{k}} D_\pi(\vec{k}) [\sin^2(k_{*1}) + \sin^2(k_{*2}) + \sin^2(k_{*3})] \\ & = \frac{g_A^2 \alpha_t^2 L^3 L_t}{4F_\pi^2} e^{-6h} XY. \end{aligned} \quad (89)$$

At $O(C)$ we have the connected bubble diagram shown in Fig. 10. If the vertex is located at lattice site \vec{n} , the lowest-order interaction is

$$e^{-12h} (e^{-C\alpha_t} - 1) c_\uparrow^*(\vec{n}) c_\uparrow'(\vec{n}) c_\downarrow^*(\vec{n}) c_\downarrow'(\vec{n}). \quad (90)$$

Summing over all sites, we find that the connected bubble in Fig. 10 has the amplitude

$$L^3 L_t e^{-12h} (e^{-C\alpha_t} - 1) Y^2. \quad (91)$$

XIII. AVERAGE ENERGY FROM SIMULATIONS

The average energy can be computed by taking $-(\partial/\partial\beta)\ln Z$ and then adding μA to the result, where A is the average number of nucleons. The partition function is given by

$$\begin{aligned} Z(\beta) & \propto e^{-2(m_N - \mu)\beta L^3} e^{(C\beta/2)L^3} \int D\pi Ds Dc' Dc^* \\ & \times \exp[-S_{\bar{N}\bar{N} + \pi\bar{N}\bar{N} + s\bar{N}\bar{N}} - S_{\pi\pi} - S_{ss}]. \end{aligned} \quad (92)$$

It is convenient to define a new partition function Z' with normalization,

$$Z'(\beta) = \int D\pi Ds Dc' Dc^* \exp[-S_{\bar{N}\bar{N} + \pi\bar{N}\bar{N} + s\bar{N}\bar{N}} - S_{\pi\pi} - S_{ss}]. \quad (93)$$

Z' is what we actually compute in the simulation. Then

$$-\frac{\partial}{\partial \beta} \ln Z = -\frac{\partial}{\partial \beta} \ln Z' + 2(m_N - \mu)L^3 - \frac{C}{2}L^3. \quad (94)$$

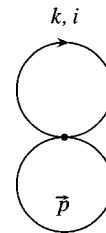
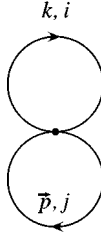


FIG. 9. Two-loop connected bubble due to a $\pi\pi\bar{N}\bar{N}$ interaction in the temporally improved action at $O(g_A^2)$.

FIG. 10. Two-loop connected bubble at $O(C)$.

After computing $-(\partial/\partial\beta)\ln Z$, we subtract out the value for $-(\partial/\partial\beta)\ln Z$ at the same β , but zero neutron density. In our theory we have not included pion self-interactions. Therefore, in the absence of neutrons we can calculate $-(\partial/\partial\beta)\ln Z$ for free pions exactly. If we later decide to include pion self-interactions, then a separate simulation with only pions will be needed for this calculation.

At zero neutron density and free neutral pions, the lattice path integral gives

$$Z' \propto Z_{pion} = \{\det[(S_{\pi\pi})_{ij}]\}^{-1/2}, \quad (95)$$

where $(S_{\pi\pi})_{ij}$ are the coefficients of the quadratic form in the pion action $S_{\pi\pi}$. We find

$$-\frac{\partial}{\partial\beta} \ln\{\det[(S_{\pi\pi})_{ij}]\}^{-1/2} = \frac{1}{2} \frac{\partial}{\partial\beta} \sum_k \ln \left[\left(\frac{m_\pi^2}{2} + 3 \right) \alpha_t + \alpha_t^{-1} - \sum_i e_i \cos(k_{*i}) \right]. \quad (96)$$

This quantity is the pion contribution to $-(\partial/\partial\beta)\ln Z'$. This is not exactly what one might define as the pion contribution to the energy, though it is closely related. To calculate the pion contribution to the energy, one also needs to add

$$\frac{1}{2} L^3 L_t \frac{\partial}{\partial\beta} \ln(\alpha_t) = \frac{1}{2} L^3 L_t \beta^{-1}, \quad (97)$$

which arises from an additional factor of

$$\left[\frac{1}{\sqrt{\alpha_t}} \right]^{L^3 L_t} \quad (98)$$

in the partition function. This factor is due to the conjugate momenta integrations going from the Hamiltonian formalism to the path integral formalism,

$$\begin{aligned} & \int dp \langle q_{n+1} | \exp \left[\frac{\Delta T}{2} \frac{\partial^2}{\partial^2 q} \right] | p \rangle \langle p | q_n \rangle \\ & \propto \int dp \exp \left[-\frac{\Delta T}{2} p^2 + ip(q_{n+1} - q_n) \right] \\ & \propto \frac{1}{\sqrt{\Delta T}} \exp \left[-\frac{1}{2\Delta T} (q_{n+1} - q_n)^2 \right]. \end{aligned} \quad (99)$$

After we calculate $-(\partial/\partial\beta)\ln Z$, we can compute the average energy per nucleon using

TABLE I. (a) $\langle a^{n_t} \leftrightarrow a^\dagger \rangle$ for $g_A=0, C=-0.135$. (b) $\langle a^{n_s} \leftrightarrow a^\dagger \rangle$ for $g_A=0, C=-0.135$. (c) E/A for $g_A=0, C=-0.135$.

(a)	n_t	0	1	2
	Free	0.7568	0.5027	0.3444
	One-loop	0.7453	0.5059	0.3537
	Simulation	0.7447(2)	0.5057(3)	0.3537(3)
(b)	n_s	1		
	Free	-0.03903		
	One-loop	-0.03940		
	Simulation	-0.03936(2)		
(c)				
	Free	6.665		
	Two-loop	6.653		
	Simulation	6.652(1)		

$$\frac{E}{A} = -\frac{1}{A} \frac{\partial}{\partial\beta} \ln[Z/Z_{pion}] + \mu. \quad (100)$$

In the simulations L_t is kept fixed, and α_t is varied in order to compute $\partial/\partial\beta$.

XIV. WEAK COUPLING RESULTS

In this section we check that the results of our numerical simulations at weak coupling agree with our results from perturbation theory. For the neutrons we define the temporal two-point correlation functions,

$$\begin{aligned} \langle a \leftrightarrow a^\dagger \rangle^{n_t} & \equiv Z^{-1} \text{Tr} \{ \exp[-(\beta - n_t \alpha_t) H] a_\uparrow(n_t, 0, 0, 0) \\ & \times \exp(-n_t \alpha_t H) a_\uparrow^\dagger(0, 0, 0, 0) \} \end{aligned} \quad (101)$$

and spatially separated correlation functions in the x direction

$$\langle a \leftrightarrow a^\dagger \rangle^{n_s} \equiv Z^{-1} \text{Tr} [\exp(-\beta H) a_\uparrow(0, n_s, 0, 0) a_\uparrow^\dagger(0, 0, 0, 0)]. \quad (102)$$

The results are exactly the same in the y and z directions. Similarly for the neutral pion, we define the temporal and spatial correlation functions

$$\begin{aligned} \langle \pi \leftrightarrow \pi \rangle^{n_t} & \equiv Z^{-1} \text{Tr} \{ \exp[-(\beta - n_t \alpha_t) H] \pi(n_t, 0, 0, 0) \\ & \times \exp(-n_t \alpha_t H) \pi(0, 0, 0, 0) \}, \end{aligned} \quad (103)$$

$$\langle \pi \leftrightarrow \pi \rangle^{n_s} \equiv Z^{-1} \text{Tr} [\exp(-\beta H) \pi(0, n_s, 0, 0) \pi(0, 0, 0, 0)]. \quad (104)$$

At weak coupling we compare the temporal and spatial correlation functions for the neutron and pion, as well as the energy per nucleon, E/A . We use the parameters $a^{-1} = 150$ MeV, $\beta = 2.0$, $L = 3$, $L_t = 3$, $m_N^{phys} = 939$ MeV, and $m_\pi^{phys} = 135$ MeV, $\mu = m_N - 0.1$. We first take $g_A = 0$ and $C = -0.135$. In Tables I(a) and I(b) we show the results for the

free neutron correlation functions, the one-loop results using the self-energy correction given in Eq. (81), and the results of our Monte Carlo simulation.

In Table I(c) we show the free neutron value for the energy per neutron, the two-loop corrected value using Eq. (91), and the result of the simulation.

There is no correction to the free pion correlation function when $g_A=0$. We see that all the simulation results match the loop calculations for $g_A=0$ and small C .

For $C=0$ and small g_A , there are two sets of diagrams that we would like to separately compare with simulation results. The temporally improved neutron action has the form

$$S_{\bar{N}N+\pi\bar{N}N} = \sum_{\vec{n},i} e^{(m_N-\mu)\alpha_i} c_i^*(\vec{n}) c_i'(\vec{n} + \hat{0}) - \sum_{\vec{n},i,j} c_i^*(\vec{n}) \times (e^{-X(\vec{n})})_{ij} c_j'(\vec{n}) - h \sum_{\vec{n},\hat{l}_s,i} [c_i^*(\vec{n}) c_i(\vec{n} + \hat{l}_s) + c_i^*(\vec{n}) c_i(\vec{n} - \hat{l}_s)], \quad (105)$$

where $X_{ij}(\vec{n})$

$$\begin{bmatrix} 6h - \frac{g_A \alpha_t}{2F_\pi} \Delta_3^\pm \pi_0(\vec{n}) & -\frac{g_A \alpha_t}{2F_\pi} (\Delta_1^\pm - i\Delta_2^\pm) \pi_0(\vec{n}) \\ -\frac{g_A \alpha_t}{2F_\pi} (\Delta_1^\pm + i\Delta_2^\pm) \pi_0(\vec{n}) & 6h + \frac{g_A \alpha_t}{2F_\pi} \Delta_3^\pm \pi_0(\vec{n}) \end{bmatrix}. \quad (106)$$

The one-loop corrected neutron correlator gets a contribution from both Eqs. (72) and (74); the one-loop corrected pion correlator uses Eqs. (83) and (85); and the one-loop corrected energy per neutron has terms (87) and (89). The comparisons with simulation results for $g_A=0.750$, $C=0$, are shown in Tables II(a)–II(e) and are labeled by “exp,” which stands for the exponential form used in the temporally improved action.

We will also remove the temporally improved diagrams which gave us the contributions (74), (85), and (89). We do this by replacing the term in the action

$$- \sum_{\vec{n},i,j} c_i^*(\vec{n}) (e^{-X(\vec{n})})_{ij} c_j'(\vec{n}) \quad (107)$$

by

$$\sum_{\vec{n},i,j} c_i^*(\vec{n}) M_{ij}(\vec{n}) c_j'(\vec{n}), \quad (108)$$

where $M_{ij}(\vec{n})$ is

$\exp(-6h)$

$$\times \begin{bmatrix} -1 - \frac{g_A \alpha_t}{2F_\pi} \Delta_3^\pm \pi_0(\vec{n}) & -\frac{g_A \alpha_t}{2F_\pi} (\Delta_1^\pm - i\Delta_2^\pm) \pi_0(\vec{n}) \\ -\frac{g_A \alpha_t}{2F_\pi} (\Delta_1^\pm + i\Delta_2^\pm) \pi_0(\vec{n}) & -1 + \frac{g_A \alpha_t}{2F_\pi} \Delta_3^\pm \pi_0(\vec{n}) \end{bmatrix}. \quad (109)$$

TABLE II. (a) $\langle a^{n_t} \leftrightarrow a^\dagger \rangle$ for $g_A=0.750, C=0$.

n_t	0	1	2
Free	0.7568	0.5027	0.3444
One-loop (lin)	0.7586	0.4978	0.3400
Simulation (lin)	0.7585(1)	0.4974(1)	0.3399(1)
One-loop (exp)	0.7496	0.5005	0.3475
Simulation (exp)	0.7494(1)	0.5000(1)	0.3472(1)

TABLE II. (b) $\langle a^{n_s} \leftrightarrow a^\dagger \rangle$ for $g_A=0.750, C=0$

n_s	1
Free	-0.03 903
One-loop (lin)	-0.03 859
Simulation (lin)	-0.03 856(1)
One-loop (exp)	-0.03 890
Simulation (exp)	-0.03 886(1)

TABLE II. (c) $\langle \pi^{n_t} \leftrightarrow \pi \rangle$ for $g_A=0.750, C=0$

n_t	0	1
Free	0.1764	0.0615
One-loop (lin)	0.1780	0.0644
Simulation (lin)	0.1780(3)	0.0643(3)
One-loop (exp)	0.1810	0.0660
Simulation (exp)	0.1809(2)	0.0659(2)

TABLE II. (d) $\langle \pi^{n_s} \leftrightarrow \pi \rangle$ for $g_A=0.750, C=0$

n_s	1
Free	0.0364
One-loop (lin)	0.0366
Simulation (lin)	0.0364(2)
One-loop (exp)	0.0367
Simulation (exp)	0.0365(2)

TABLE II. (e) E/A for $g_A=0.750, C=0$

Free	6.665
Two-loop (lin)	6.673
Simulation (lin)	6.672(1)
Two-loop (exp)	6.640
Simulation (exp)	6.638(1)

The comparisons with simulation results for this linearized action are also shown in Tables II(a)–II(e) and are labeled by “lin.” We see that all simulation results match the loop calculation for $C=0$ and small g_A

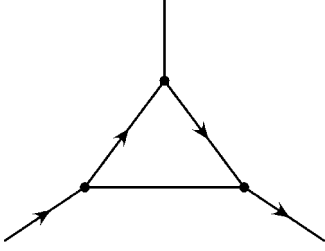


FIG. 11. One-loop correction to the one-particle irreducible $\pi\bar{N}N$ vertex.

XV. RENORMALIZATION OF COEFFICIENTS

We now discuss the renormalization of operator coefficients in our lowest-order effective Lagrangian. At zero temperature and $\mu < m_N$, the pion self-energy vanishes since there are no neutron holes. Thus, there is no renormalization for the pion wave function and mass.

In the Weinberg counting scheme, the neutron self-energy at zero temperature and $\mu < m_N$ gets a contribution from diagrams such as the one shown in Fig. 3. This is the lowest order diagram and comes at chiral order $\nu=3$. Since we require cutoff independence, the counterterm diagrams must also be at order $\nu=3$. Since this is a small correction, we will ignore wave function and kinetic energy renormalization for the neutron in the present study. Although the mass counterterm is also small, we will take some extra care with this one since we are interested in precise measurements of the energy per neutron. In the nonrelativistic formalism, the mass counterterm can be regarded as a shift in the definition of the chemical potential. Its purpose is to eliminate cutoff dependence in loop diagrams, but we will also use it to absorb residual effects due to the finite temporal spacing,

$$\alpha_t = \frac{a_t}{a} > 0. \quad (110)$$

We will refer to the mass counterterm as Δm_N . In the limit of zero neutron density, the neutrons behave as free particles. We can, therefore, calculate Δm_N in that limit. From a theoretical point of view it would be nice to measure the average energy at both zero density and zero temperature. Computationally, however, it is more practical to make the measurement at nonzero temperature.

At zero temperature and $\mu < m_N$, the one-loop contribution to the one-particle irreducible $\pi\bar{N}N$ vertex is shown in Fig. 11. This process is also at chiral order $\nu=3$. Since this is a small correction, we will also ignore the renormalization of the $\pi\bar{N}N$ coefficient and set its value to equal the physically measured value,

$$g_A \approx 1.25. \quad (111)$$

At zero temperature and $\mu < m_N$, the lowest-order contribution to the NN scattering Green's function is due to iterating the lowest-order two-particle irreducible diagrams. The lowest-order two-particle irreducible diagrams are shown in Figs. 12 and 13. When there is a bound state, or the scattering length is very large compared to other relevant scales, the

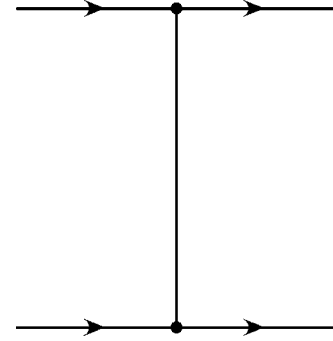


FIG. 12. Two-particle irreducible one pion exchange diagram.

two-particle irreducible kernel must be iterated and summed to all orders. The result is that the NN scattering Green's function has a cutoff dependence that cannot be regarded as a small correction. We will therefore need a nonperturbative calculation of the $\bar{N}N\bar{N}N$ contact interaction counterterm. We will use the Schrödinger equation on the lattice to deal with this problem, and we describe the procedure in the next section.

XVI. LATTICE SCHRÖDINGER EQUATION AND PHASE SHIFTS

We adjust C , the coefficient of the $\bar{N}N\bar{N}N$ contact interaction, so that the NN s -wave scattering length matches the experimental value (see, for example, [32]). In order to calculate the phase shifts, we will solve the lattice Schrödinger equation for the two-neutron system and observe the asymptotic form of the scattering wave functions. The first step will be to construct the potential between two neutrons.

Let $|0\rangle$ be the free noninteracting vacuum. The two-neutron state with zero total spatial momentum, zero total intrinsic spin, and spatial separation \vec{n}_s can be constructed as

$$|\vec{n}_s\rangle = \frac{1}{\sqrt{2L^3}} \sum_m [a_{\uparrow}^{\dagger}(\vec{n}_s + \vec{m}_s) a_{\downarrow}^{\dagger}(\vec{m}_s) - a_{\downarrow}^{\dagger}(\vec{n}_s + \vec{m}_s) a_{\uparrow}^{\dagger}(\vec{m}_s)] |0\rangle. \quad (112)$$

We let V_{2N} be the lowest-order potential in the Weinberg counting scheme between two-neutron states with zero total spatial momentum, zero total intrinsic spin, and spatial separation \vec{n}_s . Using the fact that

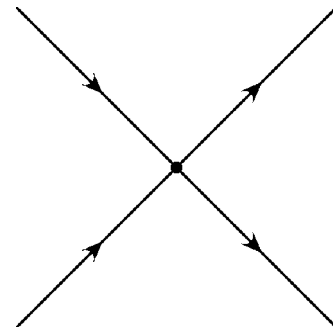


FIG. 13. Two-particle irreducible contact diagram.

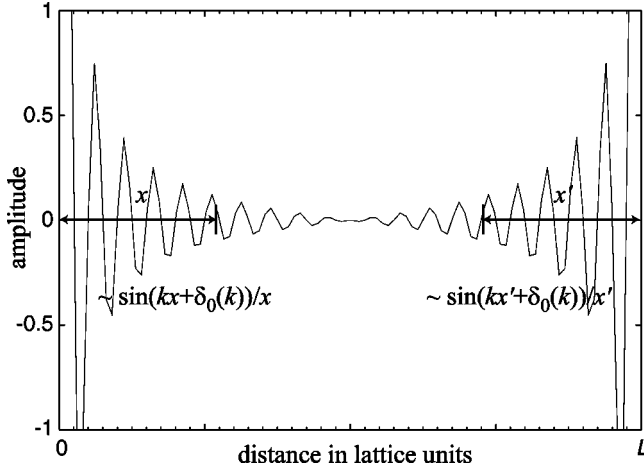


FIG. 14. Measuring s -wave phase shifts from the asymptotic form of scattering states in a periodic box of length L . The center of the potential is at $x=0$ and $x=L$.

$$\sum_{\vec{n}'_s, \vec{n}''_s} \langle \vec{n}_s | : a_{i''}^\dagger(\vec{n}'_s) \sigma_{i''j''}^s a_{j''}(\vec{n}''_s) a_{i'}^\dagger(\vec{n}'_s) \sigma_{i'j'}^s a_{j'}(\vec{n}'_s) : | \vec{n}_s \rangle = -2 \delta_{i'j', i''j''} \langle \vec{n}_s | \vec{n}_s \rangle, \quad (113)$$

we have

$$V_{2N}(\vec{n}_s) = \frac{g_A^2}{2F_\pi^2 L^3} \sum_{\vec{k}_s} \frac{e^{-i\vec{n}_s \cdot \vec{k}_s} \sum_{l_s} \sin^2(k_{s*})_{l_s}}{\frac{m_\pi^2}{2} + 3 - \sum_{l_s} \cos(k_{s*})_{l_s}} + C \delta_{\vec{n}_s, 0}. \quad (114)$$

After obtaining V_{2N} we can construct a matrix representation for the Hamiltonian in the two-neutron sector and solve the time-independent lattice Schrödinger equation. At this stage, one could implement Lüscher's formula for the measuring phase shifts in a cubical periodic box [33,34]. However, in our case we can construct the eigenvectors explicitly using Lanczos iteration, and so we find it more straightforward and accurate to read the phase shifts directly from the asymptotic forms of the s -wave scattering states. Since we are working in a periodic box, it is important to measure the phase shifts far away from the center of the potential and all its translations in the periodic box, as shown in Fig. 14.

Before using this technique for our actual neutron system, we first test our technique for hard-sphere scattering where the exact result for the s -wave phase shifts is well known. If the spheres have radii $r/2$ (therefore, the centers of the spheres are separated by r), then the s -wave phase shift has the form

$$\delta_0 = -kr, \quad (115)$$

where k is the momentum. The momentum k for a given scattering state can be determined from the energy and the free particle nonrelativistic dispersion relation. In Table III we show results for the s -wave phase shift δ_0 at inverse lattice spacing $a^{-1} = 150$ MeV, with particle masses set at m_N and a lattice volume of 20^3 . We use several radii r and show

TABLE III. Hard-sphere scattering phase shifts.

r	k	δ_0	$-kr$
4.5	0.117	-0.56	-0.53
5.5	0.147	-0.85	-0.81
6.5	0.179	-1.20	-1.16

comparisons with the exact continuum result $-kr$. The results suggest that our lattice Schrödinger technique seems to be functioning properly.

We now use the lattice Schrödinger technique to tune the coupling C to reproduce the large scattering length that is observed in nature. In Table IV we show the best fit values for C^{phys} for several different lattice spacings. We can compare this with the pionless case where the only interaction is the contact interaction. In this case we need only sum bubble diagrams, and those give the relation $C_{phys} \propto a$. The pionless calculation on the lattice has been discussed in [35].

XVII. ZONE DETERMINANT METHOD

It can be shown that fermions at inverse temperature β with spatial hopping parameter h' have a localization length [36] of

$$l \sim \sqrt{\beta h'}. \quad (116)$$

This idea was used in [37] to generate an algorithm called the zone determinant method to speed up the calculation of determinants using LU decomposition in nuclear lattice simulations.

The technique is relatively simple to describe. Let M be the neutron matrix, in general an $n \times n$ complex matrix. We partition the lattice spatially into separate zones such that the length of each zone is larger than the localization length l . Since most neutron world lines do not cross the zone boundaries, they would not be affected if we set the zone boundary hopping terms to zero. Hence, we anticipate that the determinant of M can be approximated by the product of the submatrix determinants for each spatial zone.

Let us partition the lattice into spatial zones labeled by index j . Let $\{P_j\}$ be a complete set of matrix projection operators that project onto the lattice sites within spatial zone j . We can write

$$M = \sum_{i,j} P_j M P_i = M_0 + M_E, \quad (117)$$

where

TABLE IV. C^{phys} for different lattice spacings.

a^{-1}	$C^{phys}(\text{MeV}^{-2})$
150 MeV	-4.0×10^{-5}
200 MeV	-3.4×10^{-5}
250 MeV	-3.1×10^{-5}
300 MeV	-2.9×10^{-5}

$$M_0 = \sum_i P_i M P_i, \quad (118)$$

$$M_E = \sum_{i \neq j} P_j M P_i. \quad (119)$$

If the zones can be sorted into even and odd sets so that

$$P_j M P_i = 0 \quad (120)$$

whenever i is even and j is odd or vice versa, then we say that the zone partitioning is bipartite. We now have

$$\begin{aligned} \det(M) &= \det(M_0) \det(1 + M_0^{-1} M_E) \\ &= \det(M_0) \exp\{\text{Tr}[\log(1 + M_0^{-1} M_E)]\}. \end{aligned} \quad (121)$$

Using an expansion for the logarithm, we have

$$\det(M) = \det(M_0) \exp\left\{ \sum_{p=1}^{\infty} \frac{(-1)^{p-1}}{p} \text{Tr}[(M_0^{-1} M_E)^p] \right\}. \quad (122)$$

Let us define

$$\Delta_m = \det(M_0) \exp\left\{ \sum_{p=1}^m \frac{(-1)^{p-1}}{p} \text{Tr}[(M_0^{-1} M_E)^p] \right\}. \quad (123)$$

Let $\lambda_k(M_0^{-1} M_E)$ be the eigenvalues of $M_0^{-1} M_E$ and R be the spectral radius,

$$R = \max_{k=1, \dots, n} (|\lambda_k(M_0^{-1} M_E)|). \quad (124)$$

It has been shown [38] that for $R < 1$,

$$\frac{|\det(M) - \Delta_m|}{|\Delta_m|} \leq c R^m e^{c R^m}, \quad (125)$$

where

$$c = -n \log(1 - R). \quad (126)$$

The spectral radius R determines the convergence of our expansion. R can be reduced by increasing the size of the spatial zone relative to the localization length l . In the special case where the zone partitioning is bipartite, we note that for any odd p ,

$$\text{Tr}[(M_0^{-1} M_E)^p] = 0. \quad (127)$$

In that case,

$$\Delta_{2m+1} = \Delta_{2m}. \quad (128)$$

In the simulations presented in this article we use the zone determinant method to calculate neutron matrix determinants. We use the second-order approximation Δ_2 with zones of the smallest possible size, a single spatial point ([1,1,1] in the notation of [37]). An estimate of the approximation error is discussed along with each measurement in the results section.

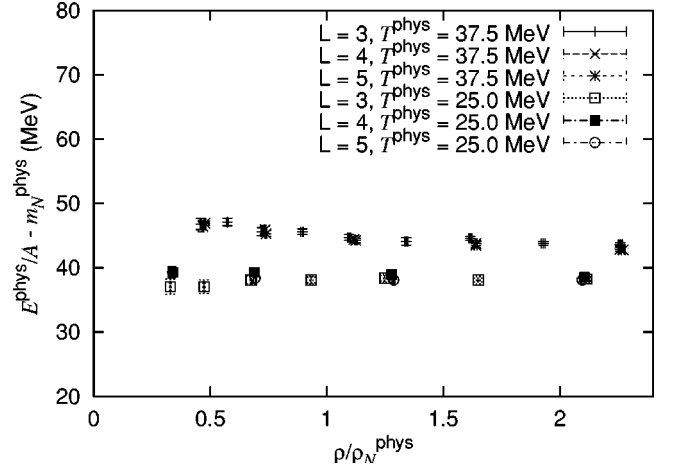


FIG. 15. Energy per neutron in MeV for temperatures 25 and 37.5 MeV and different lattice volumes. The inverse lattice spacing is $a^{-1}=150$ MeV and $\alpha_t=1.0$.

XVIII. RESULTS

We have generated simulation results for $a^{-1}=150$ MeV; $\alpha_t=a_t/a=1.0$; temperatures $T^{\text{phys}}=25$ and 37.5 MeV; and lattice sizes 3^3 , 4^4 , and 5^5 . Half-filling at this lattice spacing occurs at

$$\frac{\rho}{\rho_N} = 2.64, \quad (129)$$

where ρ_N^{phys} is the normal nuclear density of about 0.17 nucleons per fm^3 . The calculations were performed using the zone determinant method using the second-order approximation Δ_2 with zones consisting of a single spatial point. By calculating the exact determinants of some generated matrix configurations, we estimate the systemic error for the zone expansion to be about $<0.1\%$ for $T^{\text{phys}}=37.5$ MeV and $<0.5\%$ for $T^{\text{phys}}=25.0$ MeV.

We have dealt with the complex action by computing the phase as an observable,

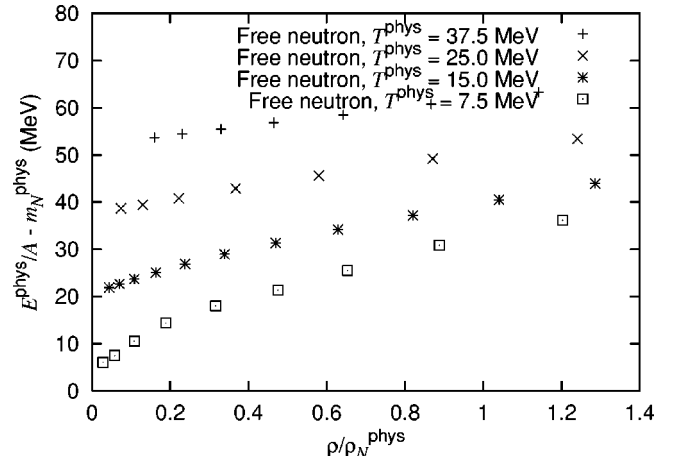


FIG. 16. Energy per nucleon in MeV for temperatures 7.5, 15, 25, and 37.5 MeV and lattice volume 4^3 . The inverse lattice spacing is $a^{-1}=150$ MeV and $\alpha_t=1.0$.

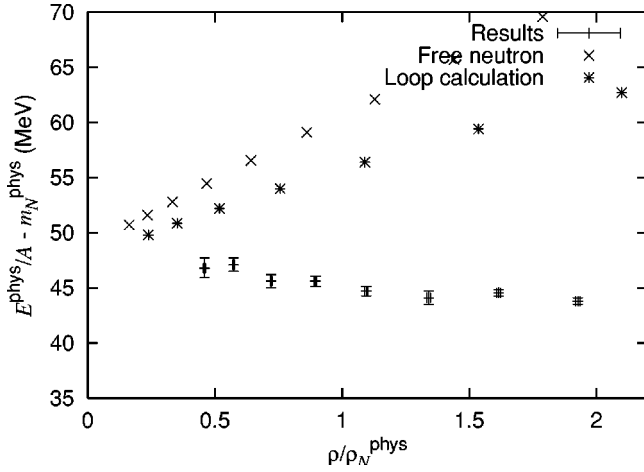


FIG. 17. Energy per neutron for temperature 37.5 MeV and comparisons with the free neutron result on the lattice and loop calculations. The inverse lattice spacing is $a^{-1}=150$ MeV and $\alpha_t=1.0$.

$$\langle O \rangle = \frac{\sum_{[n]} O[n] e^{-\text{Re } S[n]} e^{-i \text{Im } S[n]}}{\sum_{[n]} e^{-\text{Re } S[n]} e^{-i \text{Im } S[n]}}. \quad (130)$$

For the various simulations presented here, we found an average phase of about

$$\frac{\sum_{[n]} e^{-\text{Re } S[n]} e^{-i \text{Im } S[n]}}{\sum_{[n]} e^{-\text{Re } S[n]}} \sim 0.95 - 1.00, \quad (131)$$

and so this did not present a significant computational problem.

In Fig. 15 we show the energy per neutron as a function of neutron density. Our results indicate a rather flat function for the energy per neutron as a function of density. For compari-

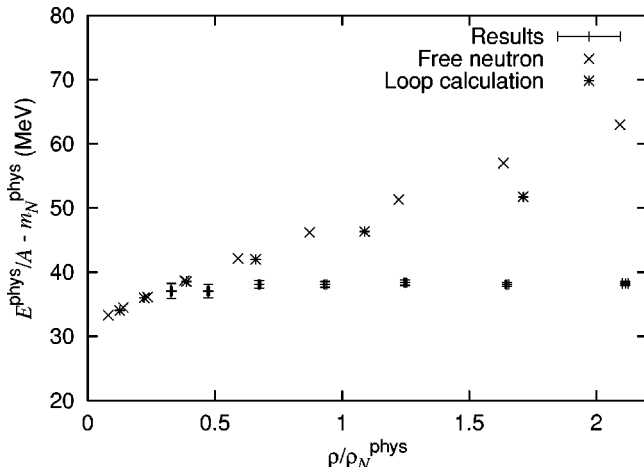


FIG. 18. Energy per neutron for temperature 25.0 MeV and comparisons with the free neutron result on the lattice and loop calculations. The inverse lattice spacing is $a^{-1}=150$ MeV and $\alpha_t=1.0$.

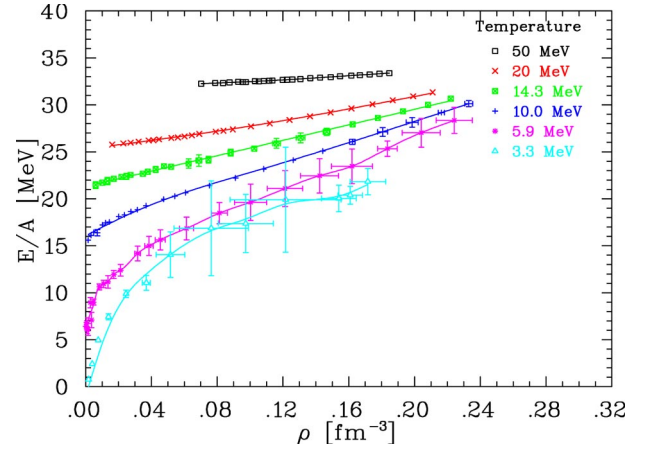


FIG. 19. (Color online) Energy per neutron vs density for various temperatures as reported in [16]. ρ_N^{phys} is at 0.17 nucleons per fm^3 . The low energy per neutron at $T=50$ MeV is likely due to lattice cutoff effects.

son we show in Fig. 16 the energy per neutron for the free neutron for temperatures $T^{phys}=7.5, 15, 25,$ and 37.5 MeV.

In Figs. 17 and 18 we compare results for free neutrons on the lattice and loop calculations for the physical values of g_A and C . As is easily seen, the loop calculations are not very close to the nonperturbative simulation results for the densities shown. This is an indication that we have a strongly coupled many-body system. This is what we expect, since the scattering length is much larger than the average separation between neutrons. This also shows why a nonperturbative calculation is necessary.

The flatness of our energy per neutron curves at these temperatures are intriguing and hopefully will be checked by others in the near future. The results of [16] also see a flattening of the energy per neutron curve with increasing temperatures (see Fig. 19). We can also compare with variational calculations [39] and recent quantum Monte Carlo results from [2]. They observe a significant flattening of the energy per neutron curve due to interactions even at zero temperature (see Fig. 20).

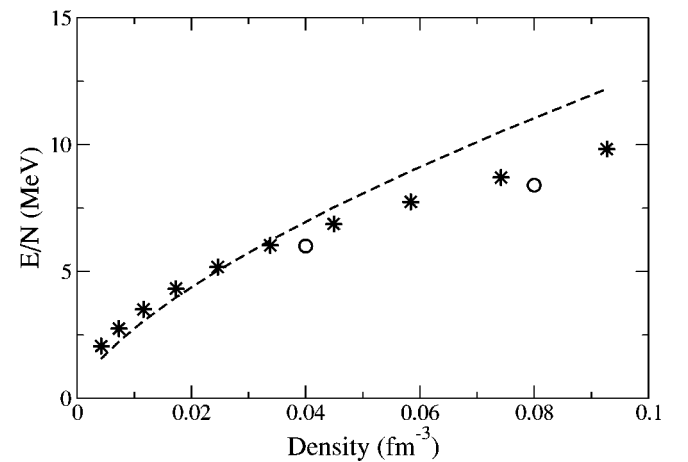


FIG. 20. Energy per neutron at zero temperature and low densities as reported in [2]. The circles are quantum Monte Carlo results from [2] and the stars are variational results from [39]. The dashed line shows one-half the result for a free Fermi gas.

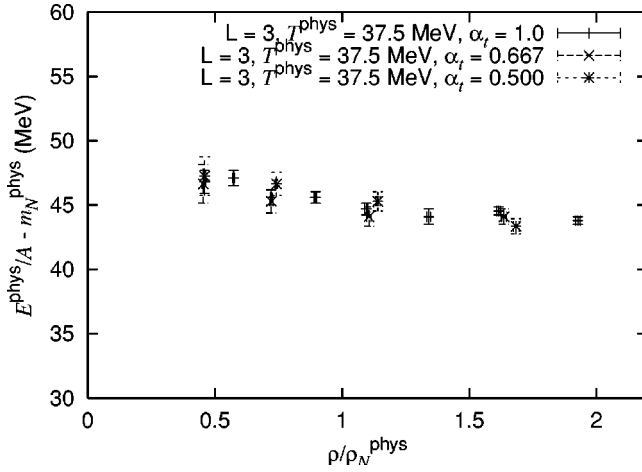


FIG. 21. Dependence on α_t for temperature 37.5 MeV. The inverse lattice spacing is $a^{-1}=150$ MeV.

We implemented a temporally improved action in order to remove as much as possible of the dependence on $\alpha_t = a_t/a$, the ratio of the temporal lattice spacing to the spatial lattice spacing. In Fig. 21 we show the dependence on α_t for $\alpha_t = 1, 0.667, 0.5$. We see that the dependence on α_t is minimal.

We now look at how the energy per neutron changes as the interaction strength is varied. According to Table IV, the physical values for C^{phys} at $a^{-1}=150$ MeV is $-4.0 \times 10^{-5} \text{ MeV}^{-2}$. If we however take the coupling to be 50%, 100%, and 150% of the physical value, we find the results shown in Fig. 22.

In Figs. 23 and 24 we show density versus chemical potential and comparisons with the free neutron and loop calculations. We can see again that loop calculations are not close to the simulation results. For fixed chemical potential, the simulation density is higher than the loop-calculated density, which is in turn higher than the free neutron density.

If our effective field theory formalism is valid, we should be able to reproduce the same results for different lattice spacings. There are, however, practical computational constraints on a . The determinant zone expansion for fixed zone

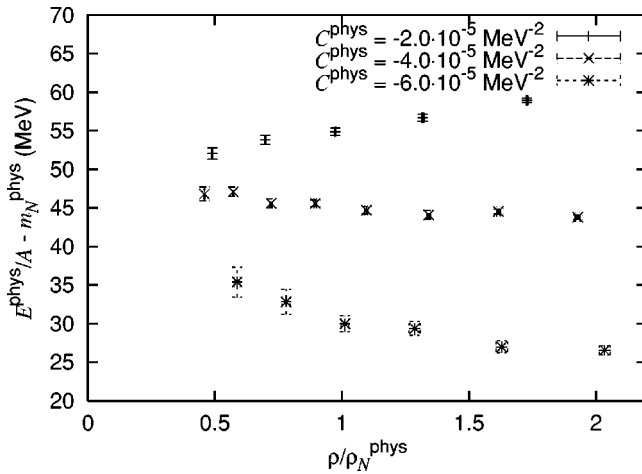


FIG. 22. Dependence on C^{phys} for temperature 37.5 MeV. The inverse lattice spacing is $a^{-1}=150$ MeV and $\alpha_t=1.0$.

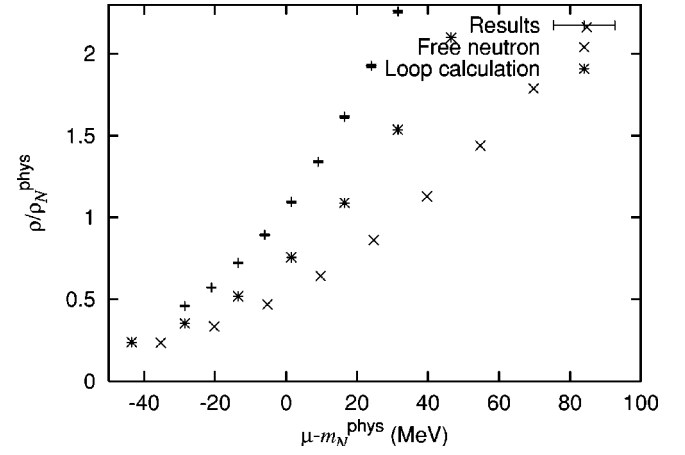


FIG. 23. Density vs chemical potential for temperature 37.5 MeV. The inverse lattice spacing is $a^{-1}=150$ MeV and $\alpha_t=1.0$.

size and expansion order will break down if the lattice spacing is too small. For $a^{-1}=200$ MeV, we estimate that the second-order approximation Δ_2 with zones consisting of a single spatial point produces errors of size roughly 3%. In Fig. 25 we compare the energy per neutron as measured for $a^{-1}=150$ MeV and $a^{-1}=200$ MeV at temperature 37.5 MeV. The results are in rather good agreement. In the future we hope to use larger zone sizes and do simulations at lattice spacings up to $a^{-1}=300$ MeV.

XIX. SUMMARY AND FUTURE DIRECTIONS

We have introduced an approach to the study of nuclear and neutron matter which combines chiral effective field theory and lattice methods. Nucleons and pions are treated on the lattice as point particles and we are able to probe larger volumes, lower temperatures, and greater nuclear densities than in lattice QCD. The low-energy interactions of these particles are governed by chiral effective field theory and operator coefficients are determined by fitting to nucleon scattering data. The leading dependence on the lattice spac-

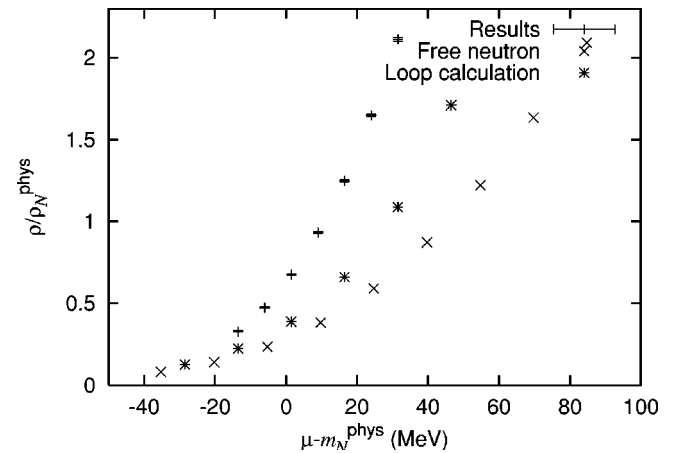


FIG. 24. Density vs chemical potential for temperature 25 MeV. The inverse lattice spacing is $a^{-1}=150$ MeV and $\alpha_t=1.0$.

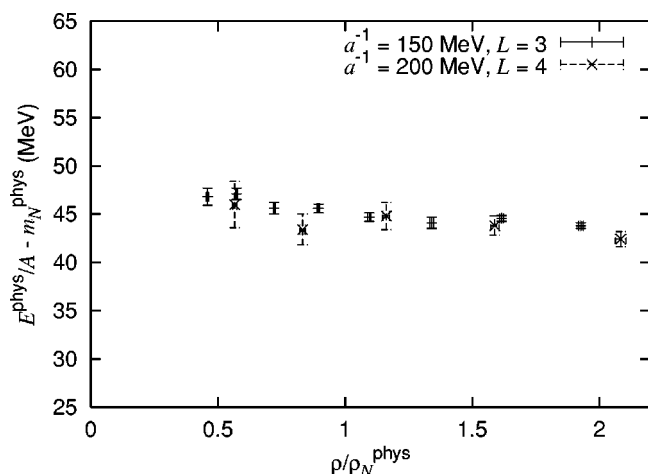


FIG. 25. Comparison of the energy per neutron results for $a^{-1} = 150$ and 200 MeV at temperature 37.5 MeV.

ing can be absorbed by the renormalization of operator coefficients. In this way, we have a realistic simulation of many-body nuclear phenomena with no free parameters, a systematic expansion, and a clear theoretical connection to QCD. We have presented results for the energy per neutron for hot neutron matter at temperatures 20 – 40 MeV and densities below twice the nuclear matter density.

In conjunction with other members of the Nuclear Lattice Collaboration, we plan several extensions, generalizations,

and improvements upon this work. In the course of producing data for this article, we have also generated a large amount of data for the neutral pion, neutron, and pair density correlation functions. This data will be analyzed and presented in a forthcoming article. In the near future we also plan to study the pionless version of the same neutron system. There has been a recent mean-field discussion of this model [40]. Without pions, the phase will be completely eliminated from the matrix determinant. This is due to the fact that the matrix is purely real, and in the Hubbard-Stratonovich formalism the up and down spins appear in a way that the matrix determinant is the square of a real number. We also plan to extend our studies to include neutrons, protons, neutral and charged pions, and make use the recent progress in implementing exact nonlinear representations of chiral symmetry on the lattice [41–44].

ACKNOWLEDGMENTS

The authors benefitted from many discussions with members of the Nuclear Lattice Collaboration and the organizers and participants of the INT Workshop on Theories of Nuclear Forces and Nuclear Systems, Fall 2003. We especially thank Boris Gelman, Ryoichi Seki, Robert Timmermans, and Bira van Kolck. This work was supported in part by U.S. DOE Grant No. DE-FG-88ER40388, U.S. NSF Grant No. DMS-0209931, and the Deutsche Forschungsgemeinschaft.

-
- [1] H. A. Bethe, *Annu. Rev. Nucl. Sci.* **21**, 93 (1971).
 - [2] J. Carlson, J. Morales, J., V. R. Pandharipande, and D. G. Ravenhall, *Phys. Rev. C* **68**, 025802 (2003).
 - [3] R. B. Wiringa and S. C. Pieper, *Phys. Rev. Lett.* **89**, 182501 (2002).
 - [4] S. C. Pieper, K. Varga, and R. B. Wiringa, *Phys. Rev. C* **66**, 044310 (2002).
 - [5] J. Carlson and R. Schiavilla, *Rev. Mod. Phys.* **70**, 743 (1998).
 - [6] B. S. Pudliner, V. R. Pandharipande, J. Carlson, S. C. Pieper, and R. B. Wiringa, *Phys. Rev. C* **56**, 1720 (1997).
 - [7] B. S. Pudliner *et al.*, *Phys. Rev. Lett.* **76**, 2416 (1996).
 - [8] S. Weinberg, *Phys. Lett. B* **251**, 288 (1990).
 - [9] S. R. Beane, P. F. Bedaque, W. C. Haxton, D. R. Phillips, and M. J. Savage, *nucl-th/0008064*.
 - [10] P. F. Bedaque and U. van Kolck, *Annu. Rev. Nucl. Part. Sci.* **52**, 339 (2002).
 - [11] N. Kaiser, S. Fritsch, and W. Weise, *Nucl. Phys.* **A697**, 255 (2002).
 - [12] M. Lutz, B. Friman, and C. Appel, *Phys. Lett. B* **474**, 7 (2000).
 - [13] R. Seki, U. van Kolck, and M. J. Savage, *Nuclear Physics with Effective Field Theory*, Proceedings of the Joint Caltech/INT Workshop, Pasadena, CA, 1998 (World Scientific, Singapore, 1998), p. 274.
 - [14] R. Brockmann and J. Frank, *Phys. Rev. Lett.* **68**, 1830 (1992).
 - [15] J. D. Walecka, *Ann. Phys. (N.Y.)* **83**, 491 (1974).
 - [16] H. M. Müller, S. E. Koonin, R. Seki, and U. van Kolck, *Phys. Rev. C* **61**, 044320 (2000).
 - [17] W. L. Qian and R.-K. Su, *nucl-th/0210008*.
 - [18] T. T. S. Kuo, S. Ray, J. Shamanna, and R. K. Su, *Int. J. Mod. Phys. E* **5**, 303 (1996).
 - [19] S. Ray, J. Shamanna, and T. T. S. Kuo, *Phys. Lett. B* **392**, 7 (1997).
 - [20] J. Pan and S. Das Gupta, *Phys. Rev. C* **57**, 1839 (1998).
 - [21] S. Weinberg, *Nucl. Phys.* **B363**, 3 (1991).
 - [22] D. B. Kaplan, M. J. Savage, and M. B. Wise, *Nucl. Phys.* **B478**, 629 (1996).
 - [23] S. R. Beane, P. F. Bedaque, M. J. Savage, and U. van Kolck, *Nucl. Phys.* **A700**, 377 (2002).
 - [24] G. P. Lepage, *nucl-th/9706029*.
 - [25] S. Weinberg, *Phys. Lett. B* **295**, 114 (1992).
 - [26] C. Ordonez, L. Ray, and U. van Kolck, *Phys. Rev. C* **53**, 2086 (1996).
 - [27] M. Creutz, *Found. Phys.* **30**, 487 (2000).
 - [28] P. Hasenfratz and F. Karsch, *Phys. Lett.* **125B**, 308 (1983).
 - [29] P. Hasenfratz and F. Karsch, *Phys. Rep.* **103**, 219 (1984).
 - [30] M. Creutz, *Phys. Rev. D* **38**, 1228 (1988).
 - [31] J. E. Hirsch, *Phys. Rev. B* **28**, 4059 (1983).
 - [32] A. Funk and H. V. von Geramb, *nucl-th/0010058*.
 - [33] M. Lüscher, *Nucl. Phys.* **B354**, 531 (1991).
 - [34] M. Lüscher, *Commun. Math. Phys.* **105**, 153 (1986).
 - [35] S. R. Beane, P. F. Bedaque, A. Parreno, and M. J. Savage, *hep-lat/0312004*.

- [36] D. Lee and P. Maris, Phys. Rev. D **67**, 076002 (2003).
[37] D. J. Lee and I. C. F. Ipsen, Phys. Rev. C **68**, 064003 (2003).
[38] I. C. Ipsen and D. Lee, "Determinant approximations," 2003.
[39] B. Friedman and V. R. Pandharipande, Nucl. Phys. **A361**, 502 (1981).
[40] J.-W. Chen and D. B. Kaplan, hep-lat/0308016.
[41] S. Chandrasekharan, M. Pepe, F. D. Steffen, and U. J. Wiese, hep-lat/0306020.
[42] B. Borasoy, R. Lewis, and P.-P. A. Ouimet, hep-lat/0310054.
[43] R. Lewis and P.-P. A. Ouimet, Phys. Rev. D **64**, 034005 (2001).
[44] I. A. Shushpanov and A. V. Smilga, Phys. Rev. D **59**, 054013 (1999).